Supplementary Material (ESI) for Soft Matter

Supporting information

Core-Shell Polymer Nanorods Prepared from Reactive Polymer Bilayer via Sequential Complete Wetting

*Jinseok Byun[a], Nam-Hyo Kim[b], Dong Hyun Lee[a], Kun-Hong Lee[b], and Jin Kon Kim,[a,] **

S1. Experimental Section

Fabrication of the AAO template: Anodized oxide aluminum (AAO) was prepared by a general two-step anodization. Prior to anodization, a highly pure aluminum sheet (99.999%, 1 mm thickness) was electropolished to decrease the roughness and remove irregularities of the surface. Electropolishing was carried out in the mixture of perchloric acid and ethanol (1:4 v/v) at 7°C, 20V, for 5min. After electropolishing, the aluminum sheet was washed with ethanol and DI water. First anodization was performed in oxalic acid (0.3M) with a platinum cathode at 15°C at 40V for over 8 h. An irregular porous thick oxide layer was etched by immersing the aluminum into a mixture of chromic acid/phosphoric acid (1.8wt% H_2CrO_4 / 6wt% H_3PO_4) at 65°C for 5 h and dimple layer remained. The second-anodization was performed for 90 s at the same condition as that of the first-anodization. Finally, the pores were widened by using 0.1M phosphoric acid at 30°C for 55 min.

Preparation of the bilayer film: PMMA-GMA with the M_w of 115,500 g mol^{-1} and PDI of 1.7, respectively, was synthesized via free radical polymerization. The functionality of GMA (the number of GMA groups per PMMA chain) is 12.5. PS-mCOOH (carboxylic acid group is attached to only one end of the chain) with the M_w and PDI being 135000 g mol^{-1} and 1.13, respectively, was purchased from Scientific Polymer Products Inc. The PMMA homopolymer with the M_w of 106,000g mol^{-1} and PDI of 1.1 (purchased from Polymer Source Inc.) was also employed to investigate the effect of the interfacial reaction on the infiltrating mechanism. PMMA-GMA layer was spin-coated onto a silicon wafer with the thickness of 100 nm from toluene solution (1 wt%, 3000 rpm) and the solvent was completely removed under vacuum for 6 h at room temperature. PS-mCOOH with a thickness of 65nm was also spin-coated from a mixed solvent (87/13 v/v) of cyclohexane and toluene (0.8 wt%, 3500 rpm), a non-solvent for the PMMA-GMA, onto the PMMA-GMA layer. The thickness of PS-mCOOH layer could be varied from 40 to 65 nm by adjusting the concentration of the solution. The procedure for the preparation of the non-reactive bilayer is the same as that of the reactive case.

Fabrication of the Nanorods: The AAO template was put onto the bilayer film with a weight of 1 kg for good contact between the AAO and the bilayer, and maintained at 180°C for 24 h for complete infiltration. To remove the AAO template, aluminum was selectively etched by $HgCl_2$ aqueous dispersion solution, and the alumina was dissolved in aqueous solution of phosphoric acid. To investigate the infiltration mechanism, the sample was quenched at given time by using liquid nitrogen.

Characterization of the morphology: To observe the of the morphology of the nanorods, the sample was coated with osmium (Osmium coater, Neoc-ST) and examined by using field emission scanning electron microscopy (FESEM, Hitachi S-4800) operated at 3 kV, 10kV. To investigate the inner morphology, nanorods were embedded into the epoxy resin, and sliced with an ultramicrotome (Lieca EM UC6). The sliced film with a thickness of 50 nm was transferred onto Cu grid and stained by ruthenium tetroxide (RuO_4), a selective staining agent for only PS, for 15 min; thus the PS phase looks dark in the images. We employed transmission electron microscope (TEM, Hitachi 7600) operated at 120kV.

The interfacial morphology of the PS-mCOOH/PMMA-GMA bilayer was investigated by atomic force microscope (AFM, Digital Instrument D3000). To expose the interface, the unreacted PS-mCOOH was removed by selective solvent of cyclohexane at 40°C for 35h. The cantilevers used for imaging were Ultralevers of high aspect ratio with a specified spring constant of 0.4 N/m.

S2. Anodized Aluminum Oxide (AAO) template

Figure S1(a) and S1(b) show the top and cross-sectional view of SEM images of the AAO templates. The diameter and height of the pore are 80 nm and 150nm, respectively.

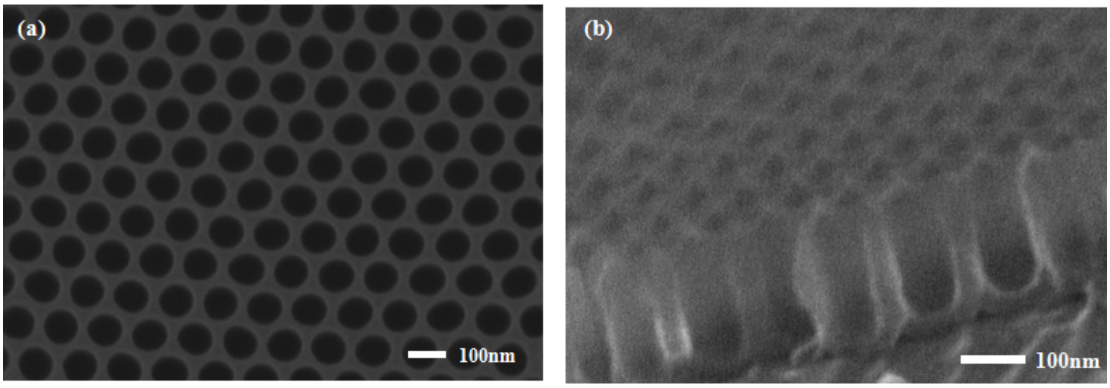

Figure S1. SEM images of (a) the top and (b) the cross-sectional view of AAO template prepared by two-step anodization.

S3. Estimation of the shell thickness from the top PS layer thickness of the bilayer

The porosity (P) of the AAO template can be obtained from Figure S2(a).

$$P = \frac{\pi}{2\sqrt{3}}\left(\frac{d}{\mathrm{D}}\right)^2 \quad (1)$$

in which D and d are the interdomain spacing and the diameter of the pores in the AAO template. From the measured values of D (100nm) and d (80nm), P is calculated to be 0.58. The total volume (V) of the PS-mCOOH nanorods inside the AAO template is determined from the thickness of the top layer ($\mathrm{H_{top}}$) of the bilayer. The thickness (t) of the shell is given in eq (2) (see Figure S2(b)).

$$\pi\left(\frac{d}{2}\right)^2 \frac{\mathrm{H}_{top}}{P} = \mathbf{V} = \pi\left(\frac{d}{2}\right)^2 \mathrm{H} - \pi\left(\frac{d}{2} - t\right)^2 (\mathrm{H} - t) \qquad (2)$$

where H is the pore length of the AAO template (150 nm).

The predicted shell thickness (t) at various thicknesses of initial top PS-mCOOH layer can be obtained from eqs (1)-(2) and given in Table S1.

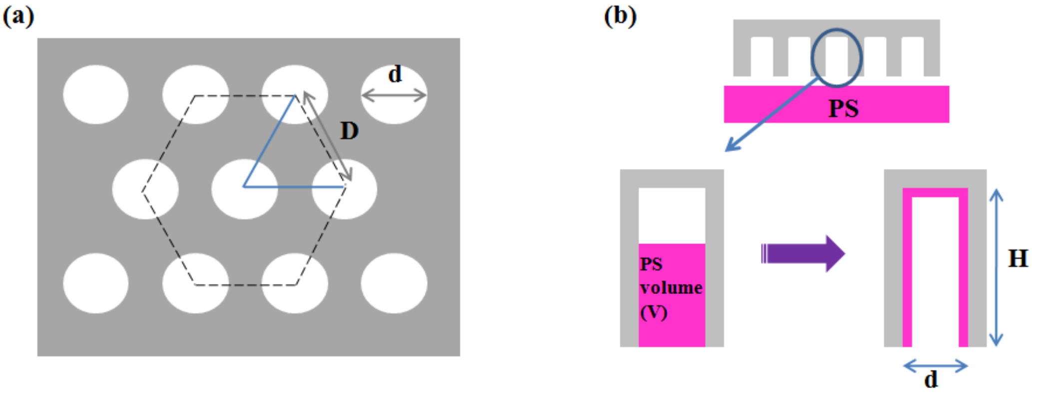

Figure S2. Schematic of (a) the bottom surface of the AAO template for the porosity calculation. d and D are the diameter of each pore and the center to center distance of the pores. (b) PS-mCOOH inside the nanopore to calculate the volume (V) and the thickness of the shell (t).

Table S1. The predicted shell thickness (t) from eq (2).

Thickness of the PS top layer of the bilayer ($\mathrm{H}_{\mathrm{top}}$)	65nm	55nm	40nm
Thickness of the PS shell of the core-shell nanorods (t)	18.5nm	14.5nm	9.5nm

S4. Roughness with increasing reaction time

Figure S3 gives AFM height images of the interface reacted for various reaction times at 180°C. After the reaction, unreacted PS-mCOOH layer was removed by selective solvent of cyclohexane. The root-mean-square (rms) roughness was obtained by AFM

(Digital Instrument). We found that the rms roughness becomes a steady value (20 nm) when the reaction time is longer than 8 h. The formation of the core-shell nanorods was only seen for an rms roughness larger than ~15 nm, corresponding to the reaction time of 5 h. On the other hand, when reaction time was shorter than 5h, the segmented pillar nanorods were formed, which is similar to non-reactive PS/PMMA bilayer.

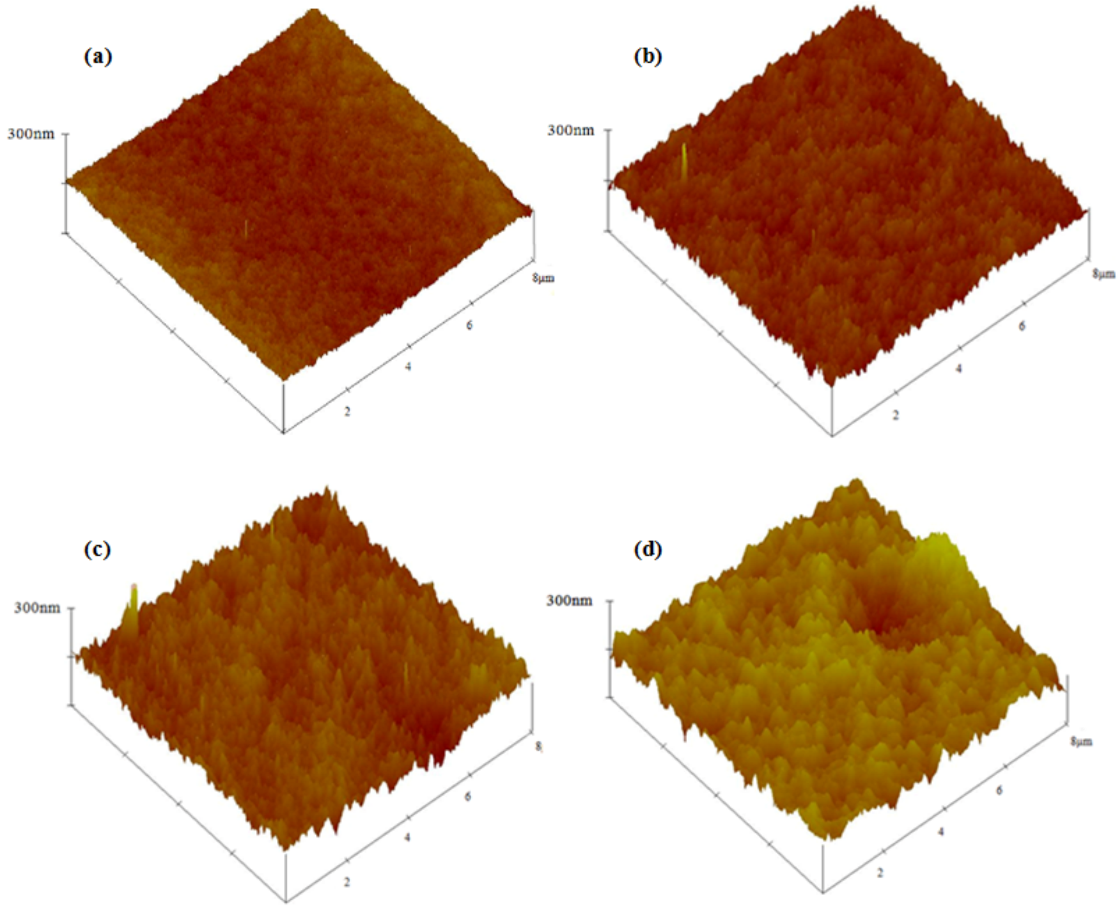

Figure S3. AFM height images of the interface reacted at 180° C for various reaction times: (a) 1 h (an rms roughness of 2nm), (b) 3 h (an rms roughness of 8nm), (c) 5 h (an rms roughness of 15 nm), and (d) 8 h (an rms roughness of 20 nm).

S5. Infiltration of another non-reactive bilayer consisting of PS and PMMA with low molecular weight

We found that the core-shell nanorods were fabricated from the reactive bilayer, whereas segmented pillar-type nanorods were formed for the non-reactive bilayer. For the non-reactive bilayer, the zero-shear viscosity (η_o) of PMMA homopolymer was 2.4 x10^5 Pa • s, which is ~30 times higher than that (8000 Pa • s) of PS-mCOOH homopolymer. Thus, a pre-made PS-mCOOH wall could be pushed up toward the top of the nanopores of AAO during the infiltration of PMMA. To investigate the molecular weight (or viscosity) effect on the infiltration mechanism for non-reactive PMMA/PS-mCOOH bilayer, we employed another PMMA with a low molecular weight (16000 g/mol) with η_o of 4500 Pa • s, which is about half of PS-mCOOH. Figure S4 shows the bottom surface image of the AAO, from which PMMA could not be infiltrated into the pre-formed PS nanotubes. Thus, the segmented pillar nanorods consisting of PS-mCOOH as the top part and PMMA as the bottom part could not be fabricated for non-reactive PS-mCOOH/PMMA bilayer when η_o of PMMA was lower than that of the PS-mCOOH.

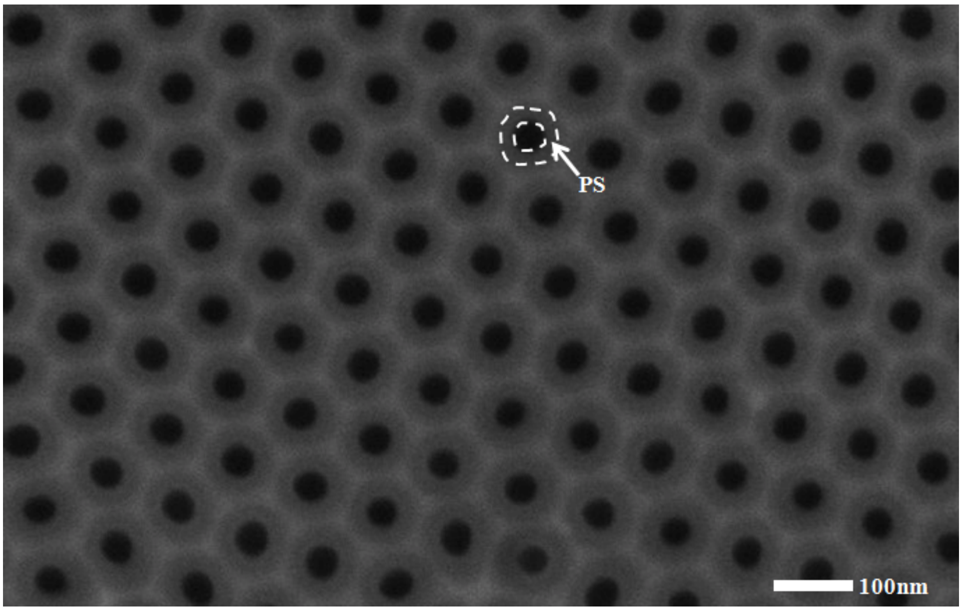

Figure S4. SEM image of the AAO bottom surface after being detached from the bilayer.